SANDIA REPORT
SAND2014-0997
Unlimited Release
Printed February 2014

A Laboratory Exposure System to Study the Effects of Aging on Super-micron Aerosol Particles

Joshua L. Santarpia, Andres L. Sanchez, Gabriel Lucero, Brandon Servantes, and Joshua Hubbard

Prepared by
Sandia National Laboratories
Albuquerque, New Mexico 87185 and Livermore, California 94550

Sandia National Laboratories is a multi-program laboratory managed and operated by Sandia Corporation, a wholly owned subsidiary of Lockheed Martin Corporation, for the U.S. Department of Energy's National Nuclear Security Administration under contract DE-AC04-94AL85000.

Issued by Sandia National Laboratories, operated for the United States Department of Energy by Sandia Corporation.

Available to DOE and DOE contractors from
U.S. Department of Energy
Office of Scientific and Technical Information
P.O. Box 62
Oak Ridge, TN 37831

Telephone: (865) 576-8401
Facsimile: (865) 576-5728
E-Mail: reports@adonis.osti.gov
Online ordering: http://www.osti.gov/bridge

Available to the public from
U.S. Department of Commerce
National Technical Information Service
5285 Port Royal Rd.
Springfield, VA 22161

Telephone: (800) 553-6847
Facsimile: (703) 605-6900
E-Mail: orders@ntis.fedworld.gov
Online order: http://www.ntis.gov/help/ordermethods.asp?loc=7-4-0#online

SAND2014-0997
Unlimited Release
Printed February 2014

A Laboratory Exposure System to Study the Effects of Aging on Super-micron Aerosol Particles

Joshua L. Santarpia, Andres L. Sanchez, Gabriel Lucero, Brandon Servantes, and Joshua Hubbard
Department 6633, Contraband Detection
Sandia National Laboratories
P.O. Box 5800
Albuquerque, New Mexico 87185-MS1148

Abstract

A laboratory system was constructed that allows the super-micron particles to be aged for long periods of time under conditions that can simulate a range of natural environments and conditions, including relative humidity, oxidizing chemicals, organics and simulated solar radiation. Two proof-of-concept experiments using a non-biological simulant for biological particles and a biological simulant demonstrate the utility of these types of aging experiments. Green Visolite®, which is often used as a tracer material for model validation experiments, does not degrade with exposure to simulated solar radiation, the actual biological material does. This would indicate that Visolite® should be a good tracer compound for mapping the extent of a biological release using fluorescence as an indicator, but that it should not be used to simulate the decay of a biological particle when exposed to sunlight. The decay in the fluorescence measured for *B. thurengiensis* is similar to what has been previously observed in outdoor environments.

CONTENTS

FIGURES AND TABLE

Nomenclature

ACC	Aerosol Capacitance Chamber
BtK	Bacillus thurengiensis Kurstaki
BSL	BioSafety Level
CBW	Chemical-Biological Warfare
CFD	Computational Fluid Dynamics
DOE	Department of Energy
DTRA	Defense Threat Reduction Agency
MATLAB	Matrix Laboratory
MD	Maryland
NOx	Mono-nitrogen oxides
N-S	Navier-Stokes
OAF	Open Air Factor
PTFE	Polytetrafluoroethylene
RH	Relative Humidity
SNL	Sandia National Laboratories
SOA	Secondary Organic Aerosol
UV	Ultraviolet
UV-APS	Ultraviolet Aerodynamic Particle Sizer

1. INTRODUCTION

To understand the fate of any aerosol in the atmosphere and assess the impacts or hazards they pose, the atmospheric processes that affect the physical, chemical and biological properties of airborne particulate matter must be characterized. For instance, the viability/toxicity and the fluorescence of Chemical-Biological Warfare (CBW) agents and simulants released into the open atmosphere decay at vastly different rates as compared to those enclosed in conventional laboratory apparatus due to atmospheric chemical interactions and compounds, termed open-air factors (OAF). Because CBW agents cannot be studied outside, there are very few open-air decay rates to inform operational hazard prediction models. Further, there is little understood about the effects of OAF on the biological detection signatures for agents. Past and current studies indicate that the specifics of how long a biological attack may be detectable by current technologies are presently unknown. Tracers used to simulate the transport of CBW agents, and validate models, often rely on Ultraviolet (UV) fluorescence for detection. The fluorophores in the tracer material may also be subject to the same degradation processes that affect CBW agents and stimulants. Finally, the radiative and hygroscopic properties of both anthropogenic and naturally occurring super-micron aerosol particles (such as dusts and bacteria) are critically important to understanding earth's climate processes. Laboratory measurements of these properties after known aging processes are relatively non-existent.

In order to understand the fate of chemical and biological aerosols intentionally released into the environment, the potential respiratory transmission of some diseases, the atmospheric processes that affect the physical, chemical and biological properties of airborne particulate matter must be carefully studied and understood. There have been a small number of papers regarding what has been called the Open Air Factor (OAF) (Dark and Nash, 1970; Cox et al., 1973) that have attempted to describe the inexplicable loss of viability of certain organisms when released into the environment. This work has indicated that this OAF may be caused by the interaction of atmospheric ozone and terpenes that produce lower vapor pressure products that can condense to form surface monolayers toxic to many of the organisms studied. These are the same reaction processes which form secondary organic aerosol (SOA) involved in photochemical smog formation, and which may affect the optical properties of ambient dusts. These processes have not been studied in the gas-phase or at atmospherically relevant oxidant concentrations. The hygroscopicity of the aerosol has also been shown to play a significant role in the fate of an aerosol due to changes in its susceptibility to certain chemical processes (Santarpia, et al., 2012). In order to understand the roles of atmospheric interactions in the fate of hazardous aerosol in the atmosphere, continued studies of these effects is necessary.

Rotating drum aerosols chambers have been used for several decades to study the behavior of super-micron aerosol particles under varying atmospheric conditions (e.g. Goldberg, et al., 1958; Gruel, et al., 1972). However, most of these drum designs do not allow for the observation of atmospheric chemical processes at realistic atmospheric concentrations due to their construction. In recent years some efforts have been undertaken to develop chemically inert chambers for this type of study, but the efforts are currently in their infancy and have focused on limited chemistry (Santarpia et al., 2012). This effort will focus on the development of instruments and methods suitable to study a wide range of atmospheric processes

(photochemistry, SOA formation and atmospheric oxidation processes) on Biosafety Level (BSL)-1 biological agent surrogates as well as tracer materials. In addition, these methods could be used to study the aging of aerosols and chemical processes that are important to climate process (dust particles and bacteria related to the water cycle).

2. METHODS

2.1. System Design

The first phase of this project developed an improved experimental apparatus to study aging under controlled conditions. In this way, the natural aging of aerosol under a variety of simulated ambient conditions could be studied in such a way that the physical, chemical and biological aging processes can be studied and isolated from one another. No current system in use has the capability to look at all of the proposed chemistry.

Several important modifications to a typical rotating drum design were implemented for these studies. First and foremost, in order to study chemical interactions at chemical concentration relevant to atmospheric trace-gas levels, a chemically inert drum design is needed. Past attempts at fabricating the entire drum from inert material (Santarpia et al., 2012) have been problematic due to the inadvertent generation of static charge during the rotation of the drum. Pan et al. (2013) used a Teflon-coated stainless steel drum in order to mitigate this affect, which is the approach that was taken in this study. This process is relatively common in chemical pipes. Further, other drum materials that are involved in rotation were selected to insure that no plastic on plastic contact is made during rotation, in order to limit the generation of charge. The Teflon coating will ensure that the reaction vessel is truly inert to both ozone and the volatile organic compounds. A chamber volume of 400 L was used to ensure that there is ample volume for intermittent sampling throughout the aging experiments, which in these experiments lasted several hours. Acrylite OP4 windows were used on either end of the drum to allow UV light to be introduced from the ends of the drum. In order to maintain the concentrations of gas-phase species on the interior of the drum during a long reaction, the design incorporates an inner and outer axel design where the outer axle was constructed out of a Teflon-coated, perforated, stainless steel tube wrapped in a Gore filtration membrane. This will allow gas exchange across the membrane, without the loss of aerosol. In this concept, gas concentrations are typically generated and maintained in a control loop that passes through the outer axle in order to maintain the gas-concentrations inside the drum. UV intensity was measured inside the drum prior to the start of experiments. Figure 1 shows the overall design of the laboratory system including: aerosol generation, relative humidity and ozone generation, rotating drum design and aerosol measurement.

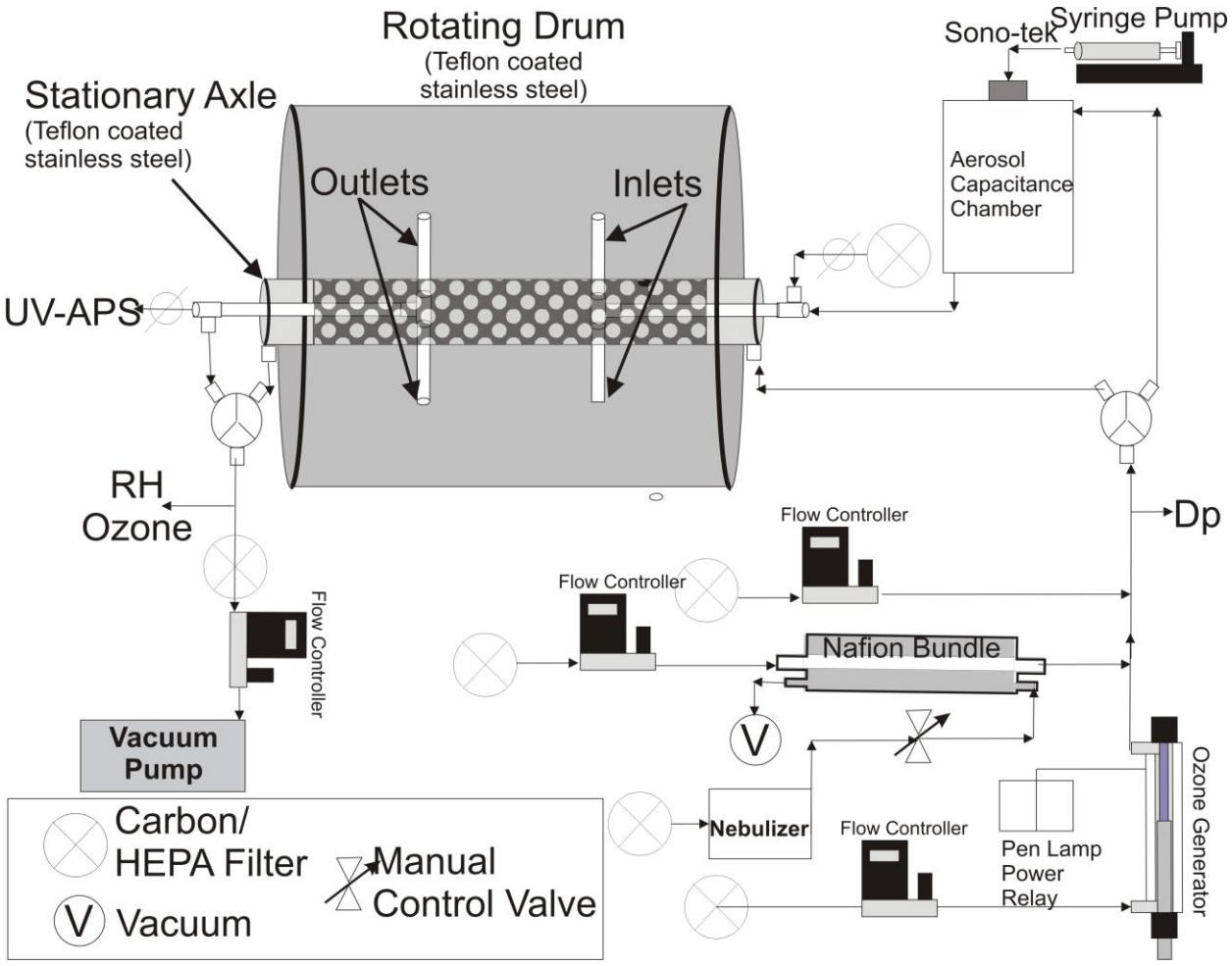

Figure 1. Schematic of the rotating drum. The scale of the axel relative that of the drum is exaggerated to show the details of the air and aerosol flow paths, and different monitors.

2.1.1 Humidity Control

In the proof of concept experiments, ambient laboratory humidity was used, but the system can control humidity in the drum using the relative humidity subsystem that was designed. In cases where humidity control is desired, humidity in the system air flow is controlled using a Nafion tube. Nafion allows the passage of water vapor, but not air, across the membrane, allowing the modification of the humidity of the sample air, without introducing any contaminants that might be present in the water into the system. In this design, similar to the Santarpia et al. (2005) design for humidifying tandem differential mobility analyzers, air of a controlled humidity is passed through the sheath air of the Nafion tube bundle in the opposite direction of the sample air. Water vapor crosses the membrane humidifying the sample air. The ratio of dry air to saturated air (coming from a humidification system) in the sheath, is varied based on an Relative Humidity (RH) measurement at the outlet of the drum to achieve the desired RH inside the drum (Figure 2).

2.1.2 Aerosol Generation

Aerosol is generated using an ultrasonic spray nozzle (Sono-Tek Corp., 06–04010), with a 30-mL syringe and pump (Sono-Tek Corp., 11-01061) set to infuse the liquid suspension at a rates of 100 μL/min and 1 mL/min. The broadband ultrasonic generator (Sono-Tek Corp., 06–05108), used to control the nozzle frequency, is set to 3W. The nozzle of the Sono-Tek is placed at the top of an aerosol capacitance chamber (ACC) that allows for mixing and initial evaporation of the droplets (initially 18 μm diameter) prior to their entering the drum. The aerosol was introduced into the drum from the ACC at a flow rates between 5 and 10 Standard Liter Per Minute.

2.1.3 Ozone generation

In the proof of concept experiments, no ozone was generated to allow observations of aerosol aged only by the simulated solar radiation. By introducing precursor gasses, ozone could be created in a similar manner to tropospheric ozone trough the photolysis of mono –nitrogen oxides (NOx) by the simulated solar radiation; however, ozone may also be generated directly when it is necessary to separate the affects of UV radiation and ozone. In order to generate ozone directly, a small mercury pen lamp (Pen Ray, 97-0067-01) was placed outside the drum and shielded by a Teflon body with ports for air flow across the lamp. The mercury lamp produces UV light with energy sufficient to photolyze oxygen (wavelengths less than 220 nm). The singlet oxygen formed recombines with molecular oxygen (O_2) to form ozone. The arrangement can be seen in Figure 2.

2.1.4 Solar Simulation

In order to completely understand the aging of aerosol in the ambient environment using a laboratory test system, it is necessary to simulate solar radiation. In the atmosphere, solar radiation is the driving force behind the generation of oxidant species such as ozone and many radical species. Radiation at certain wavelengths (primarily UV) can also directly interact with aerosol particles to modify their properties. Most gas-phase atmospheric chemistry and observed interactions with aerosol particles occurs at UV (below 450 nm) wavelengths, therefore in order to understand the effects of solar radiation in this context, the laboratory system must attempt to simulate the UV spectrum of the sun observed at the earth's surface. Many commercial systems use arc-xenon lamps for this simulation; however, these lamps are extremely expensive and most solar simulation systems are designed for much smaller applications. A less expensive alternative is the metal halide lamp. Metal halide lamps are recommended to simulate clear spring and summer skies in hydroponics applications (Figure 3).

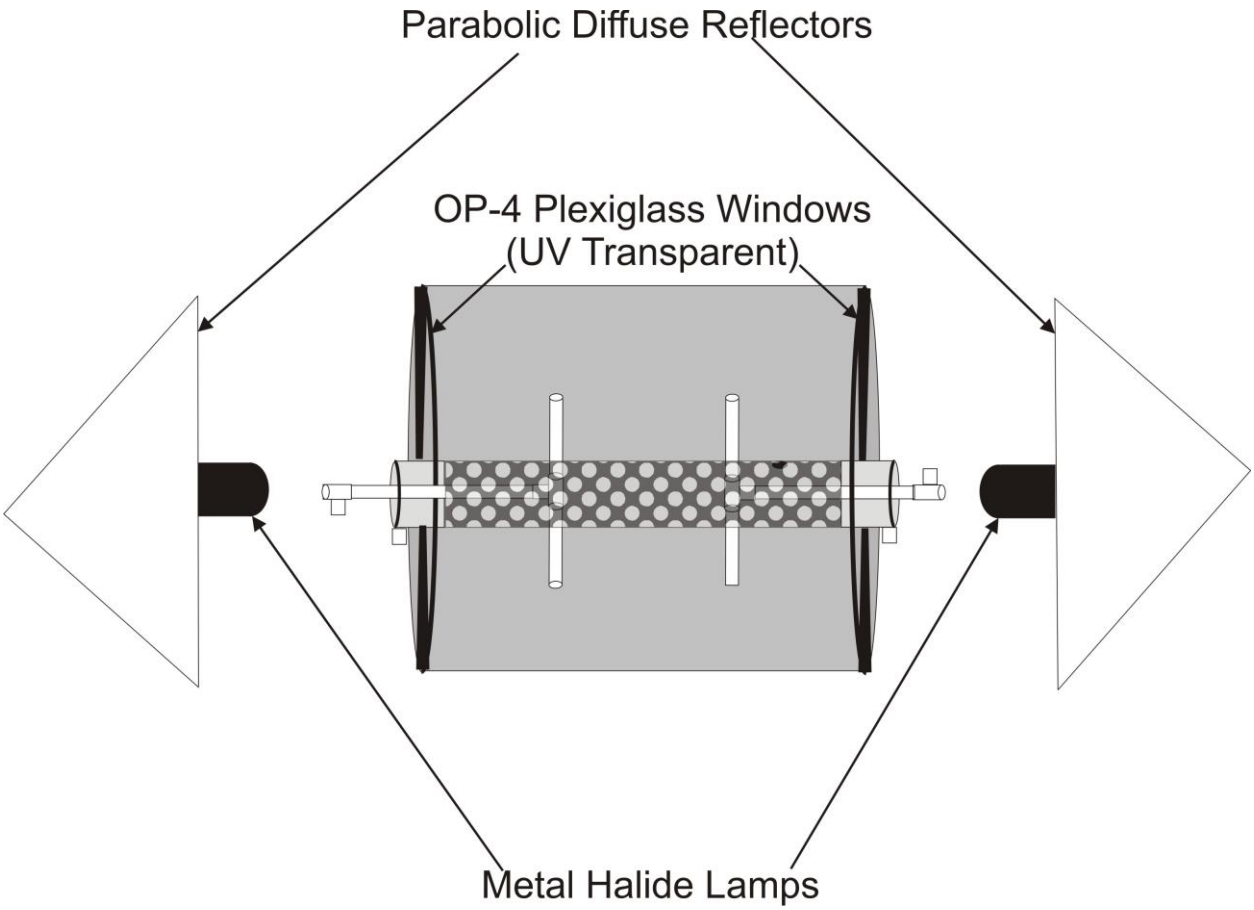

Figure 2. Schematic of the UV exposure system showing the rotating drum, the metal halide lamps, parabolic diffuse reflectors and the Acrylite OP4 windows.

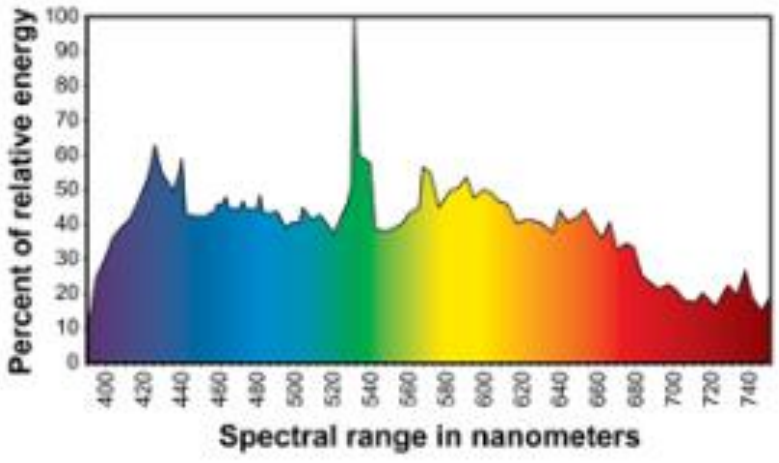

Figure 3. Spectrum of a metal halide lamp from manufacturer's literature.

In order to ensure that radiation is spread as evenly as possible over the interior of the drum volume, two metal halide lamps reflected on parabolic diffuse reflectors are directed into the drum from either end. The parabolic reflectors are made from 0.25" thick expanded Polytetrafluoroethylene (PTFE) sheets adhered to a metal parabolic reflector. Expanded PTFE has been shown to have nearly 100% reflectance of -UV wavelengths (Figure 4) at thicknesses of several millimeters.

As stated before, this UV light is allowed to pass into the drum through 3, 0.125" thick Acrylite OP4 windows located on each end of the drum. At this thickness, the manufacturer specifications indicate that approximately 90% of the UV in the wavelength range of interest (between 360 and 400 nm) will be allowed to pass into the drum. Having lamps at both ends of the drum reduces the intensity variation across the length of the drum and produces a parabolic light intensity with local maxima at the ends of the drum and a minimum at the center.

2.1.5 Rotating drum

The rotating drum developed and used in this study consists of a ~400L stainless steel tube capped on each end with stainless steel ends. Each end has 3 Acrylite OP4 windows, to allow penetration of UV light, for simulated solar exposure. A stainless steel perforated tube serves as the center axle of the drum. This axle is fixed, allowing the drum to rotate around it by means of a sealed bearing system attached to the end-caps of the drum. This center axel is covered by an expanded PTFE membrane, allowing the trace gasses to be exchanged between the hollow axel and the interior of the drum. This allows trace gasses (ozone, water vapor and organics) to be replenished during long exposure experiments without disrupting air flow, and therefore aerosol, in the drum. All interior steel surfaces are coated with a thick layer of Teflon to prevent the steel from reacting with the gas-phase species in the drum. Tubing and wiring for instrumentation pass into and out of the drum via sealed ports at the end of the axel. The inlet supplies conditioned aerosol laden air into the drum. The outlet has ports connecting tubing to the UV-APS, the ozone monitor, any additional sampling equipment, and the purge pump. Each of these pumps is connected in series after a high-efficiency particulate absorption filter to prevent any aerosol from reaching the pump or being exhausted.

2.1.6 Ultraviolet Aerodynamic Particle Sizer (UV-APS)

The Ultraviolet Aerodynamic Particle Sizer (UV-APS, TSI, 3314) is commercially available system used for real-time monitoring of bioaerosol size and fluorescence. To help examine the effects of ozone on bioaerosols, a UV-APS is used to measure the aerodynamic particle size distribution and integrated fluorescence (between 430 and 580 nm) intensity distribution excited by a 355-nm laser. Sampling from the drum was limited to 1 Lpm by attaching only the inner, sample-flow inlet to the drum and letting the instrument pull the sheath air (4 Lpm) from the surrounding laboratory.

2.2. Modeling Drum Performance

An analysis of drum performance was conducted to complement experimental drum characterization. The traditional Goldberg drum has no inner cylinder whereas the SNL rotating

drum has a co-axial cylinder with no rotational velocity. The objectives of this modeling task were the following: (1) assess the probability of flow instabilities that might lead to Taylor-Couette flow and alter particle residence time, (2) to model the actual drum geometry with computational fluid dynamics to compare the internal flow field to previously published works, and (3) calculate particle residence times in the current drum geometry.

2.2.1 Couette Flow Instabilities

Couette flow is laminar flow in between parallel plates or circular cylinders. If conditions are right, instabilities may occur leading to the formation of other flow patterns. The work of Andereck, Liu, and Swinney (1986) mapped the flow patterns which result from various boundary conditions. Their work characterized the fundamental phenomena observed as early as Rayleigh (1916) and Taylor (1922). For a fixed inner cylinder, R_i=0, we see that Couette flows result for all rotational velocities of the outer cylinder (Figure 4). This is the case for the SNL rotating drum. However, if the drum had a rotating inner cylinder, flow patterns might be produced from varying the inner and outer rotational velocities. This may enhance, or reduce, particle residence times.

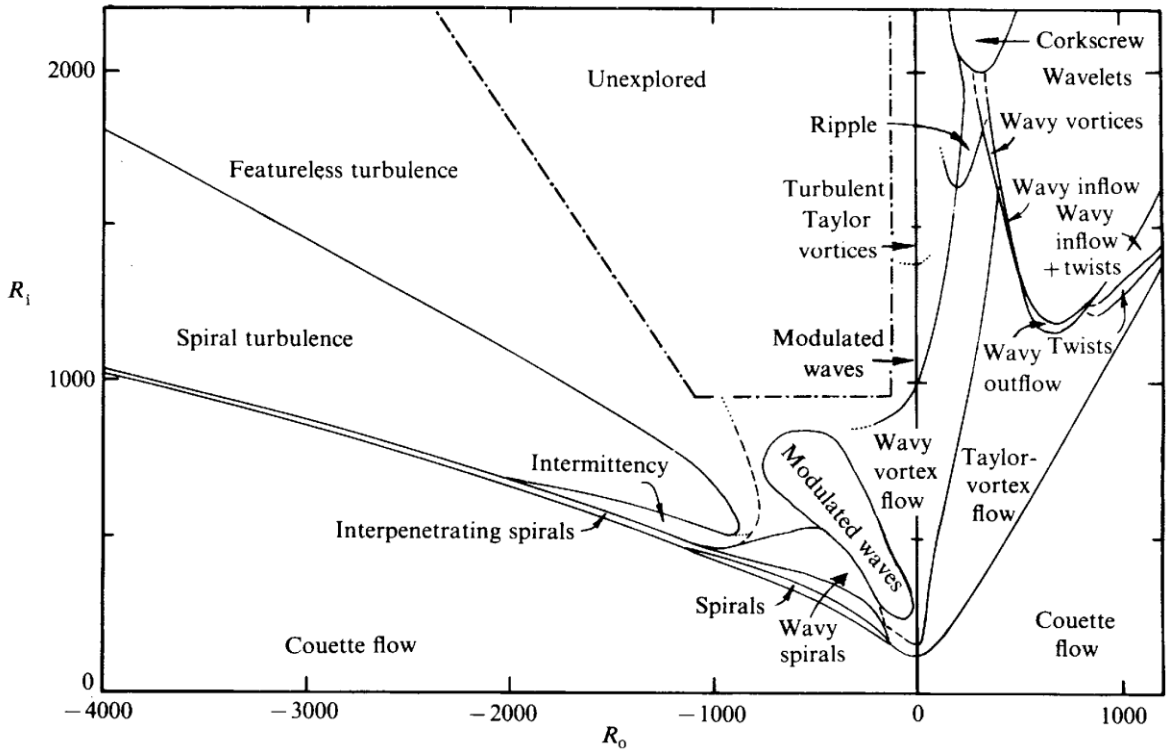

Figure 4. Map of Couette flow regimes as a function of inner and outer diameter Reynolds numbers, R_i and R_o, taken from Andereck, Liu, and Swinney (1986).

2.2.2 Analytical Solution to Velocity Profile

The works of Lapple and Shepherd (1940), Kriebel (1961), Gruel et al. (1987), and Asgharian and Moss (1992) utilize the linear velocity approximation within the Goldberg rotating drum. The angular air velocity, V_θ, is given by

$$V_\theta = \omega R_2 \left(\frac{r - R_1}{R_2 - R_1} \right) \tag{1}$$

where ω is the rotational speed of the drum, R_1 and R_2 are the inner and outer drum radii, and r is the radial coordinate. By writing the Navier-Stokes (N-S) equations in cylindrical coordinates we arrive at an Euler-Cauchy equation,

$$r^2 \frac{d^2 V_\theta}{dr^2} + \frac{dV_\theta}{dr} - V_\theta = 0\,, \tag{2}$$

which gives a different solution with respect to equation (1),

$$V_\theta = \frac{\omega R^2}{(R_2^{\,2} - R_1^{\,2})} \left(\frac{r - R_1^{\,2}}{r} \right). \tag{3}$$

Angular air velocities calculated from equations (1) and (3) are shown in Figure 5. The linear approximation results in errors between 10-30% when the radius is less than 0.1 meters for the SNL rotating drum. There is negligible error between the two velocity profiles above 0.2 meters. The N-S velocity profile will be used to obtain the most accurate particle residence times in the SNL rotating drum.

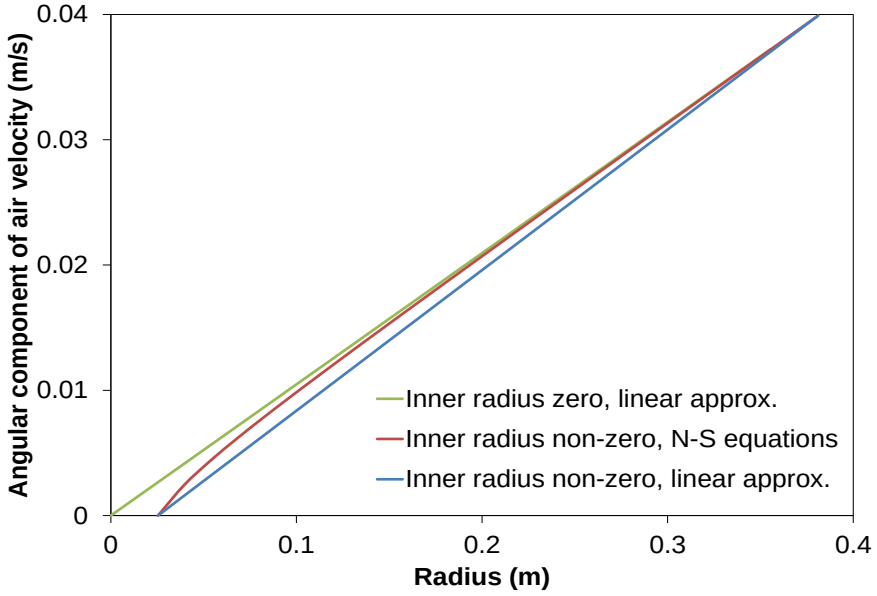

Figure 5. Angular component of air velocity as a function of drum radius for (a) an inner radius of zero using the linear velocity profile assumption, (b) a non-zero inner radius solving the N-S equations in cylindrical coordinates, and (c) a non-zero inner radius using the linear velocity profile assumption.

2.2.3 Computational Fluid Dynamics Model

A computational fluid dynamics (CFD) model was setup to evaluate the effects of aerosol inlet and outlet tubes on the viscous flow established within the cylinder. A rotational speed of 1 revolution per minute was used for these simulations. The model geometry is shown below (Figure 6) where the aerosol injection/exhaust tubes extend out to their as-built dimensions. Simulations were also performed when the injection/exhaust tubes were cut to 25% of their as-built lengths. The radial lines in the geometry show the effect of domain partitioning in ANSYS FLUENT. Parallel computing was used to speed up the computation. Twelve partitions are shown, but twenty-four partitions were used in the actual simulation.

In the full-length injection/exhaust tube model, the mesh had 18 million cells. Inflation layers were used along the tube walls to enable attempts at Large Eddy Simulation in the future. This could enable good resolution of Couette flow instabilities, e.g., vortices, if Reynolds Averaged Navier Stokes flow simulations did not predict the flow instabilities that are possible. Model parameters are given in Table 1.

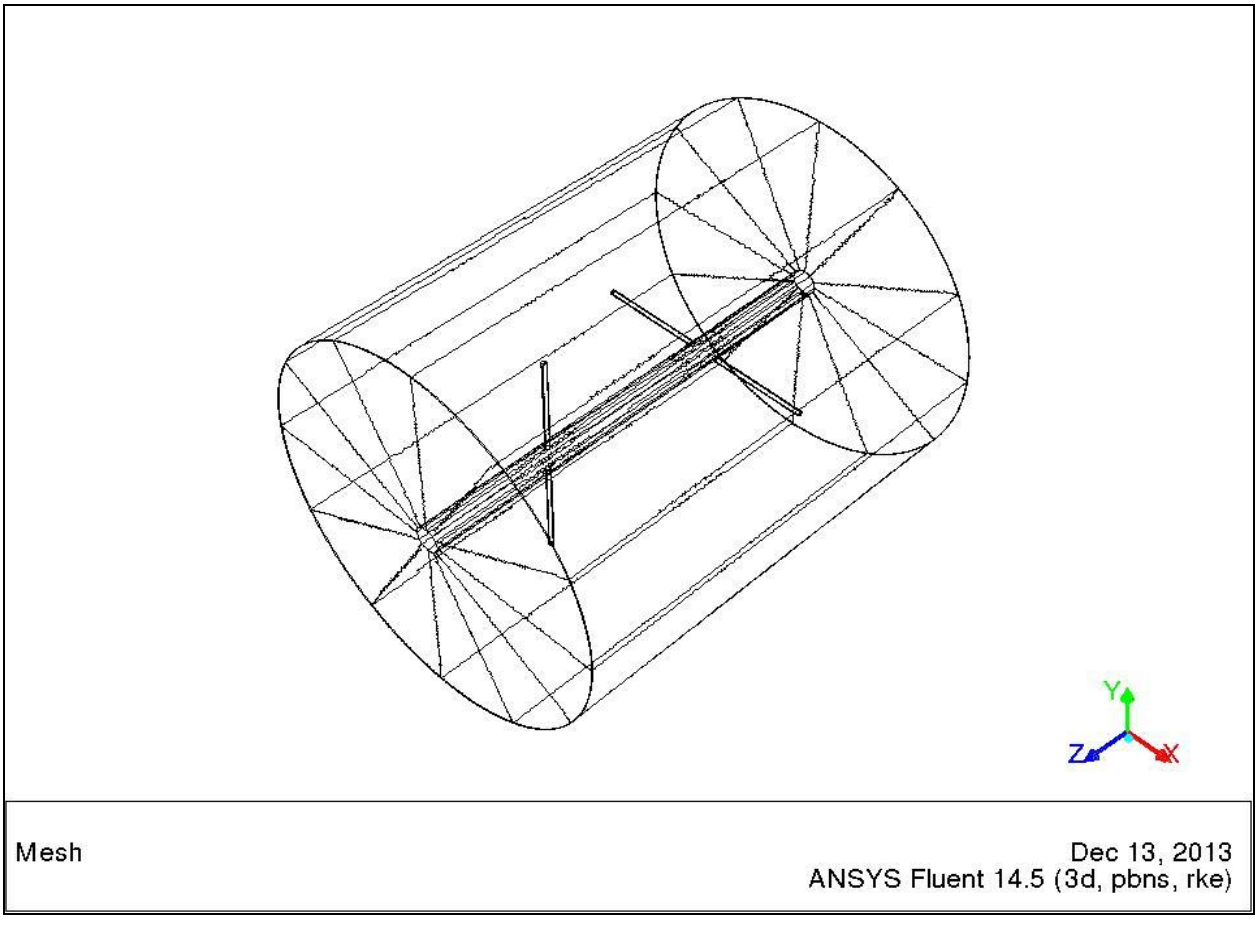

Figure 6. ANSYS FLUENT model geometry used to simulate the fluid dynamics with the SNL rotating drum.

Table 1. ANSYS FLUENT Model Parameters

	Full-length inlet/exhaust tubes	Quarter-length inlet/exhaust tubes
Mesh	18.5M	5.6M
Turbulence	Realizable k-ε, enhanced wall function	Realizable k-ε, enhanced wall function
Cell Zone Operating Conditions	Specified operating density 0.98 kg/m^3	Specified operating density 0.98 kg/m^3
Inlet air boundary condition	Mass-flow inlet, 8.17e-5 kg/s, turbulent intensity 2.5%, hydraulic diameter 0.009525 m	inlet-vent, zero gage pressure, turbulent intensity 2.5%, hydraulic diameter 0.009525 m
Outlet air boundary condition	Pressure-outlet, target mass flow 8.17e-5 kg/s, turbulent intensity 2.5%, hydraulic diameter 0.009525 m, zero gage pressure	velocity-inlet, velocity magnitude -0.595 m/s, turbulent intensity 2.5%, hydraulic diameter 0.009525 m
Wall drum boundary	moving wall, absolute rotational motion, 0.105 rad/s, no slip, other walls no slip boundaries	moving wall, absolute rotational motion, 0.105 rad/s, no slip, other walls no slip boundaries
Monitors	integral wall shear stress, inlet and outlet mass flow rate, volume integral turbulent kinetic energy, residuals	inlet and outlet mass flow rates, inlet and outlet pressures, residuals

Velocity profiles, and velocity contours, are shown in Figure 7, Figure 8, Figure 9, and Figure 10, where the former are for as-built injection/exhaust tubes, and the latter two figures are for quarter-length tubes Velocity profiles at the wall (end caps) follow the linear approximation since the end cap rotates at fixed velocity. However, we see that the velocity profile is non-linear at various axial positions. This is due to the presence of the injection/exhaust tubes as well as the nonlinearity of the N-S flow field solution.

The velocity contour plots show that the velocity profile is disturbed following the injection/exhaust tubes. At the top of each contour plot the injection/exhaust tube is not shown in the contour plane, the tubes are rotated by 90 degrees. At the leading edge of the tubes the velocity profile is closer to the steady state solution (without tubes present). The tubes disturb the flow since it is only driven by viscous forces, and 90 degrees downstream of the tube the flow disturbance is high. The flow disturbances do not protrude as deeply in to the flow field for the quarter-length tube design.

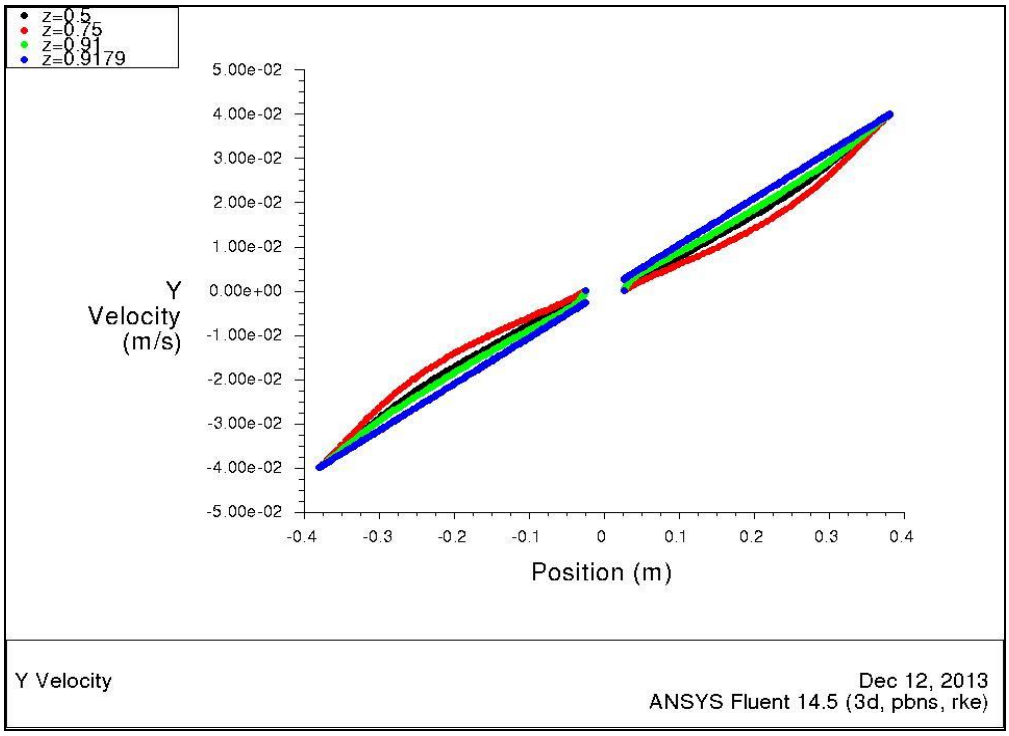

Figure 7. Full length inlet/exhaust tubes: Y-velocity profiles along the axis of the rotating drum where 0.9179 m is equivalent to the rotational speed of the endcap.

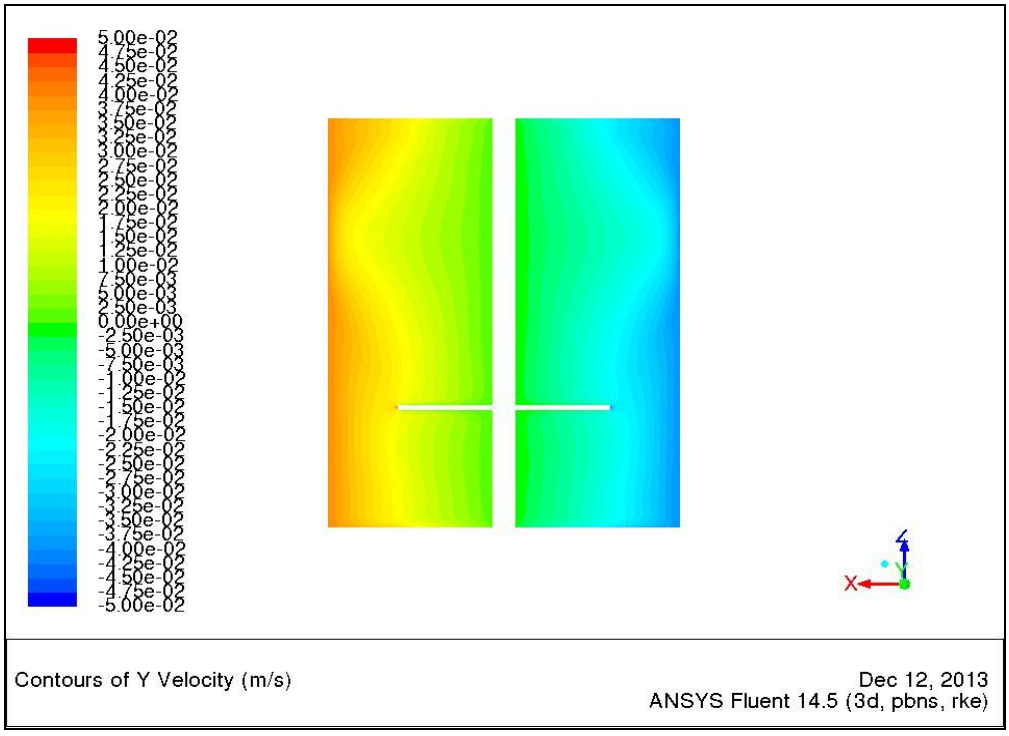

Figure 8. Full length inlet/exhaust tubes: Y-velocity contours on a plane normal to the y-axis.

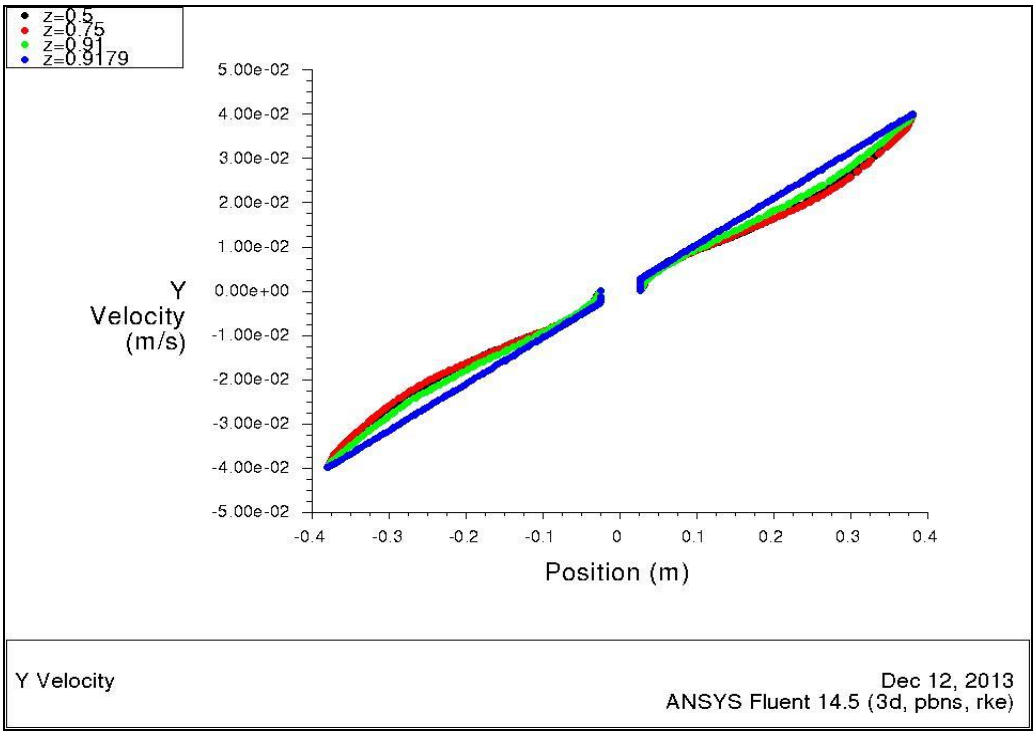

Figure 9. Quarter length inlet/exhaust tubes: Y-velocity profiles along the axis of the rotating drum where 0.9179 m is equivalent to the rotational speed of the endcap.

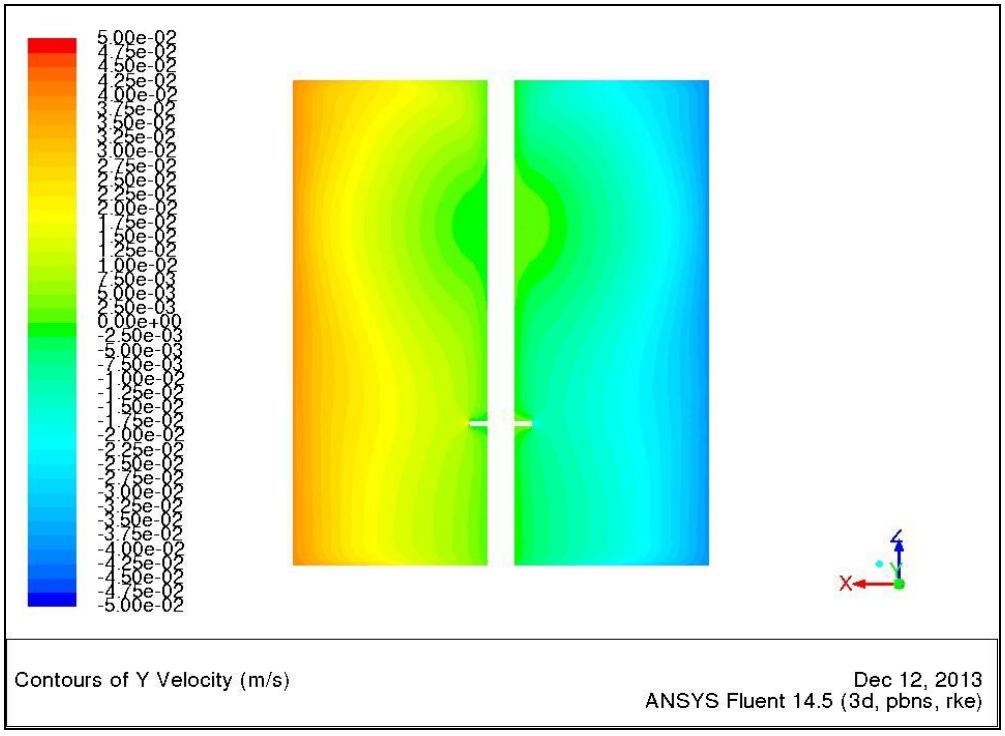

Figure 10. Quarter length inlet/exhaust tubes: Y-velocity contours on a plane normal to the y-axis.

2.2.4 Particle Trajectories and Residence Time

Calculations of particle trajectories could be performed in CFD. However, simpler methods exist to determine the residence time of particles in the rotating drum as used by Gruel et al. (1987) and Asgharian and Moss (1992). Including gravitational forces, the equations of motion in Cartesian coordinates (x , y) are given by the following:

$$\begin{aligned} \tau\ddot{x} + \dot{x} - \omega y &= 0 \\ \tau\ddot{y} + \dot{y} + \omega x + \tau g &= 0 \end{aligned} . \tag{4}$$

In equation (4), τ is the particle relaxation time given by

$$\tau = \frac{\rho_p d_p{}^2 C_c}{18\eta} , \tag{5}$$

where ω is the angular velocity of the rotating drum, g is the gravitational constant, ρ_p is particle density, d_p is particle diameter, C_c is the Cunningham slip correction factor, and η is the dynamic gas viscosity. The reader is referred to Gruel et al. (1987) for a derivation of equation (4).

Equation (4) was written as set of first order, coupled, ordinary differential equations. A non-stiff explicit Runge-Kutta formula in MATLAB was used to numerically solve the particle equations of motion. To verify the accuracy of the computation, numerical solutions were compared to the approximate analytical solutions of Gruel et al. (1987).

$$\begin{aligned} x &= e^{\tau\omega^2 t}\left[\left(x_c + \frac{\tau g}{\omega}\right)\cos\omega t + y_c \sin\omega t\right] - \frac{\tau g}{\omega} \\ y &= e^{\tau\omega^2 t}\left[y_c \cos\omega t - \left(x_c + \frac{\tau g}{\omega}\right)\sin\omega t\right] \end{aligned} . \tag{6}$$

Terminal settling velocities of 1 and 10 micrometer particles were also used to verify the code in the absence of drum rotation. For the rotational verification case, the following input parameters were used:

- particle diameter: 10 μm,
- initial location: $x_c = y_c = 0.2325$ m,
- particle density: 1 g/cc,
- angular velocity: 1 rev/min,
- and gravity was included.

The initial position was chosen such that particles hit the wall at an early time. The numerical procedure terminates the computation when the particle location is at the wall. Analytical and numerical solutions are shown in Figure 11. We should also note that the relative and absolute error tolerances of the MATLAB solver were set to 1e-7 and 1e-12, respectively, to

obtain MATLAB solutions with a relative difference less than 0.001 with respect to the analytical solution. These solutions suggest that the analytical solution presented by Gruel et al. (1987) are sufficient for estimating particle residence times in this drum.

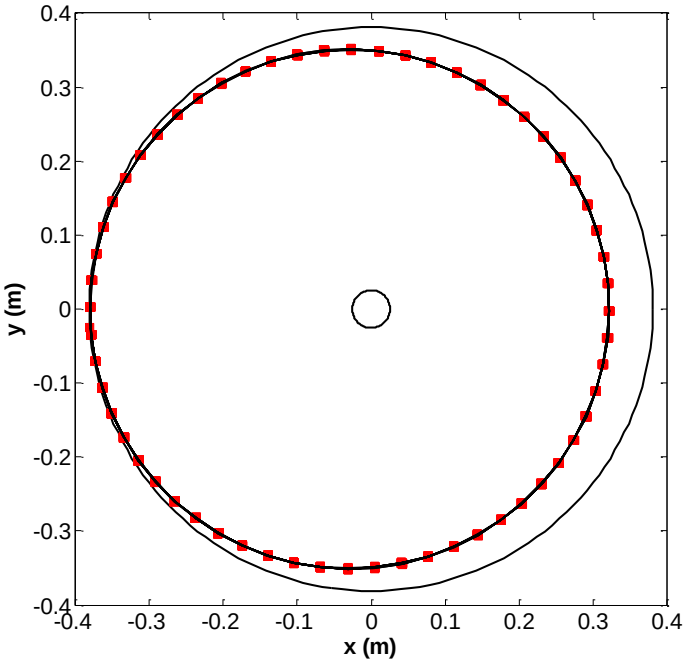

Figure 11. Particle trajectories used to verify correct execution of the MATLAB script. Red symbols represent the MATLAB ODE solution, and the black line represents the approximate analytical solution of Gruel et al. (1987).

2.3 Methods for Proof of Concept Experiments

Several proof of concept experiments were performed to expose aerosol to relevant ambient conditions in this new apparatus. Experiments focused on photobleaching of aerosol using simulated ambient sunlight, due to a lack of experimental data present in the literature. Specifically, photobleaching experiments included the aging of *Bacillus thurengiensis* spores under simulated solar UV conditions to determine if the simulated UV exposure could replicate the observed loss of fluorescence that has been observed in ambient environments and the exposure of fluorescent biological tracers, in this case Visolite® powder, to the same simulated light to examine photobleaching processes that may impact past, current and future tracer studies. Photobleaching experiments utilized the UV-APS, which excites single aerosol fluorescence at 355 nm and measures an integrated fluorescence over the visible spectrum. Bleaching was determined by the reduction in fluorescence intensity measured by the UV-APS. Past experiments in outdoor environments (author's unpublished data) have indicated that such bleaching might be very rapid for biological particles at high UV intensities (minutes), and reasonably fast (less than 2 hours) at even moderate UV intensities.

2.3.1 Preparation of samples

BtK was obtained from Dugway Proving Ground, as a dry powder. This powder was resuspended at between 1 and 5 mg/mL in distilled water and deionized (DI) water for aerosolization in the Sono-Tek. Green Visolite® powder was also resuspended at between 1 and 5 mg/mL in DI water for aerosolization. These suspensions were loaded into syringes with magnetic stir bars for aerosolization with the Sono-Tek ultrasonic nozzle. The magnetic stir bars help to keep the suspensions well mixed during aerosol generation, which improves the consistency of the aerosol distribution that is generated.

2.3.2 Measurement protocol

Each measurement period lasts between one and four hours, depending how rapidly the particle concentration and particle fluorescence is depleted. Aerosol is generated and introduced into the chamber for 10-30 minutes to reach a particle concentration of approximately 10-300 particles/cm^3. Once the aerosol has reached the desired concentration, initial measurements are made with the UV-APS and the UV lights are turned on. The UV-APS samples for 3-5 minutes approximately every 30 minutes, with all air flow stopped between sampling periods. Air lost to sampling is balanced with dry air sent into the drum. When measurements are not occurring, no air is introduced to or removed from the drum.

3. PROOF OF CONCEPT EXPERIMENTS

3.1 Characterization of UV Intensity and Temperature inside the drum

The intent of the metal halide lamps and diffuse reflectors is to mimic the UV irradiance of the sun near the earth's surface. The average solar constant at the earth's surface is between 1000 and 1100 W/m^2, integrated across all wavelengths. The fraction of that light that is in the -UV is generally about 3%, yielding 30 to 33 W/m^2 of -UV solar radiation reaching the surface of the earth. Figure 12 shows the UV irradiance across the length of the interior of the rotating drum. This would indicate that particle in the drum would receive between approximately 10 and 20 W/m^2 of UV radiation inside the drum, or between about 33% and 66% of the UV fraction of the average solar constant. The UV portion of the spectrum produced by the metal halide lamps is also spectrally similar to solar radiation. This indicates that the solar simulation should be representative of aging in natural sunlight, although somewhat less rapid than average, due to the lower output. A second set of lamps could be added to increase the maximum intensity, and the irradiance could be varied by increasing the distance of the lamps from the drum windows to provide a wider range of irradiance, if required by future experiments.

Producing a representative amount UV light comes at the cost of increasing temperature inside the drum. In particular, the interior surfaces of the drum are coated in a black Teflon to minimize the interaction of these surfaces with the reactive chemicals that will be used and could be produced in future experiments. This surface is very absorbing and can cause significant increases in air temperature in the drum, which needed to be addresses. Unmitigated, the addition of UV light to the drum caused temperature increases of the interior air temperature of between 20 and 25 degrees F. In order to control the temperature, a small portable air conditioner is used to blow humid air over the exterior surface of the drum while it rotates. When the air conditioner in operated air temperature increases were limited to 10 degrees F, above ambient, which is acceptable for simulating outdoor conditions.

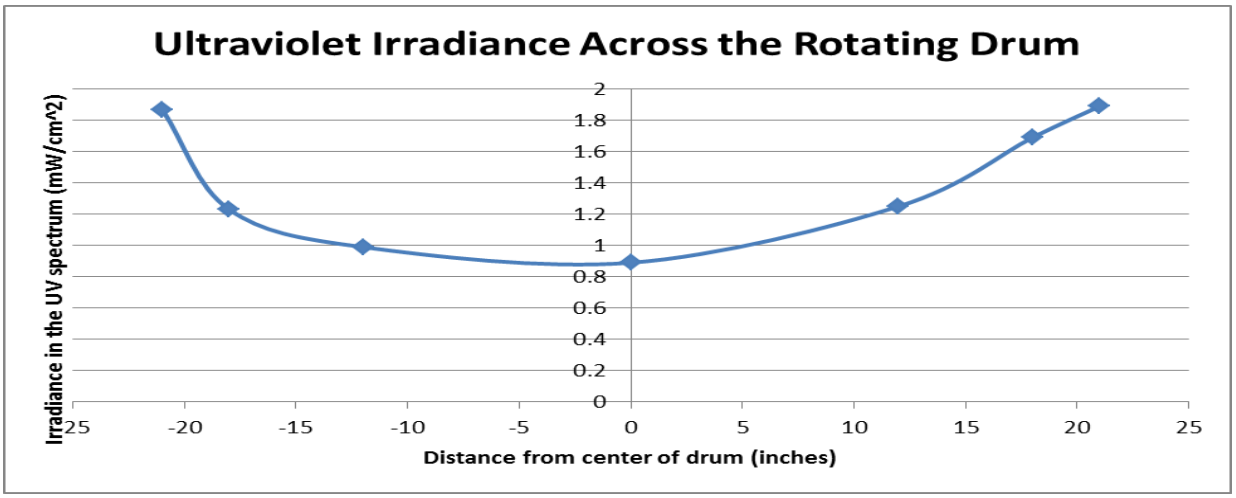

Figure 12. Ultraviolet irradiance across the rotating drum.

3.2 Photobleaching Experiments with Visolite® Tracer Aerosol

Visolite® is a common material used to find leaks in building filtration systems. It has also been used for many years as a simulant for biological aerosol particles in large-scale releases (both indoor and outdoor) where it would be impossible to release an actual biological particle. One of the reasons that it is useful as a biological simulant is that it fluoresces when excited by light in the 350-360 nm range, similar to biological particles. Figure 13 shows a three dimensional plot of the particle size distribution and fluorescence (observed by the UV-APS) of the green Visolite® used for these experiments. The measurement was taken near the end of aerosol generation during the UV exposure experiment. The peak of the aerosol distribution is approximately at the 1.197 micron bin of the UV-APS. The particle fluorescence intensity begins to saturate the UV-APS detector at around 1.7 microns.

For the purposes of examining the decay in fluorescence over time, the mean concentration weighted fluorescence was calculated in the 1.197 micron bin and tracked over the course of measurements when particles were exposed to light from the metal halide lamps to simulate solar exposure and with the lights off. Results of these calculations are shown in Figure 14. Based on these measurements, it is unlikely that the fluorescence of Visolite® is affected by exposure to UV. Although the final measurement after 73 minutes of exposure shows a drop in the mean fluorescence, the increase in the standard deviation is indicative of the variability of the fluorescence measurements at this time period, so this apparent decrease may be artificial. In fact, as particle concentrations in the drum drop over the period of the measurements, the noise in the average fluorescence calculations increases significantly, due to sampling errors with the UV-APS, at the 10 second accumulation rate used in these measurements. Future measurements would likely benefit from higher starting particle concentrations, better optimized drum parameters to further increase particle retention over time and longer accumulation times for UV-APS measurements.

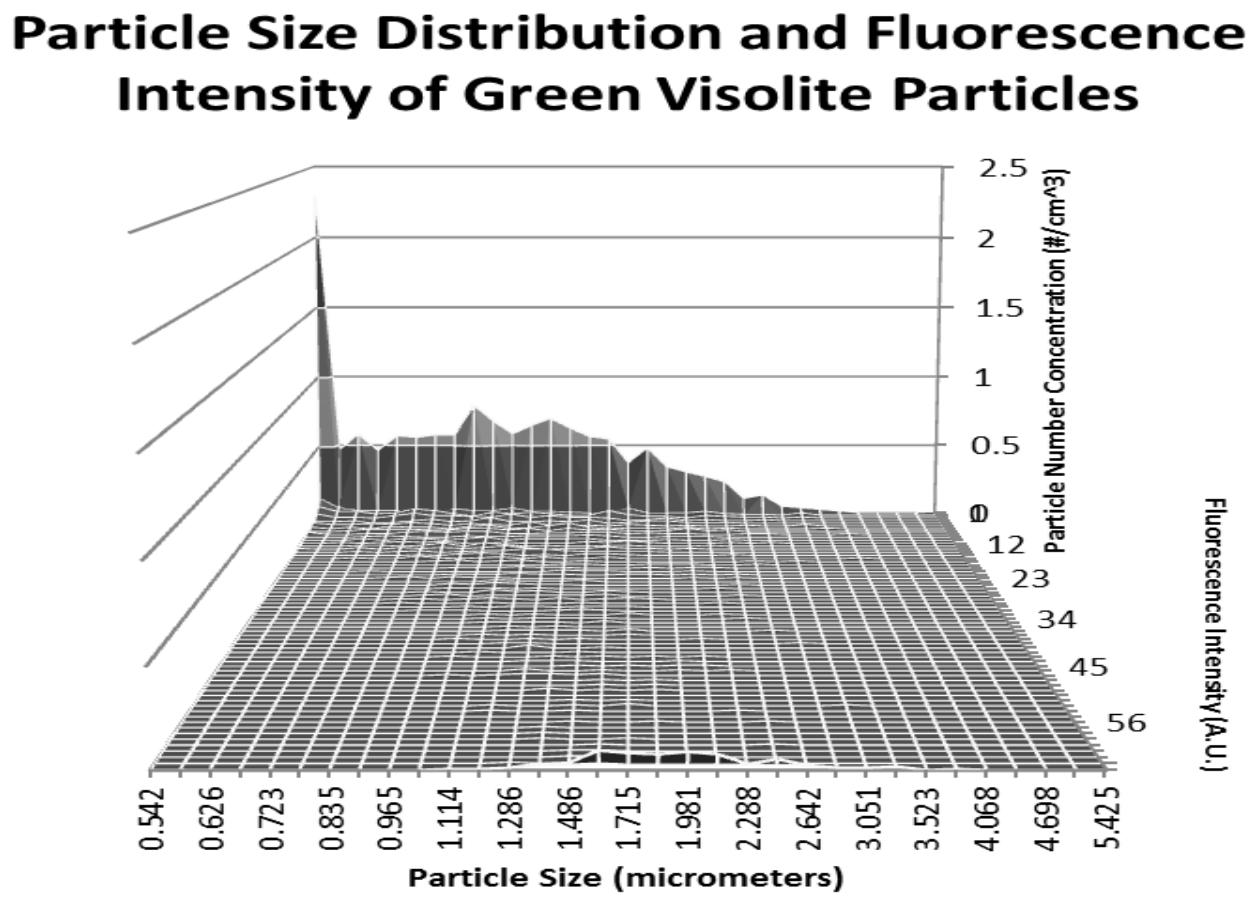

Figure 13. Aerosol number distribution and size resolved integrated fluorescence intensity as measured by the UV-APS for Green Visolite® particles.

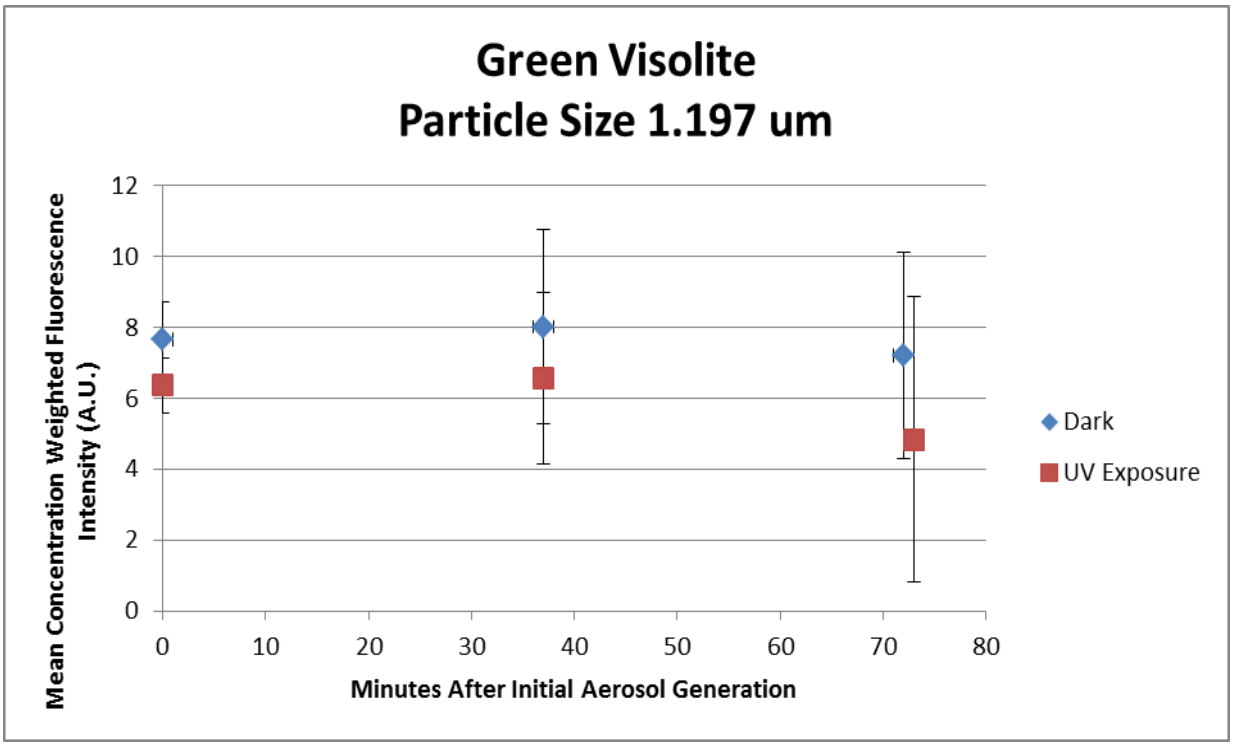

Figure 14. Fluorescence of Green Visolite after exposure to simulated sunlight in the rotating drum. Although the fluorescence appears to drop in the final timepoint at around 73 minutes of exposure the noise in the data prevent this from being a significant result.

3.3 Photobleaching Experiments with *Bacillus thurengiensis* Kurstaki Aerosol

Bacillus thurengiensis Kurstaki is one of the most common simulants for *Bacillus anthracis* in biodefense research. It shares much of its genome sequence in common with *B. anthracis*, primarily lacking the virulence plasmids. More commonly, *B. thurengiensis* is used as a biological pesticide, primarily for gypsy moths. Its high degree of similarity to *B. anthracis*, yet relative safety of use, makes it a very common simulant for biodefense research in the laboratory, and to some degree in outdoor environments. Its fluorescent properties are also very similar to *B. anthracis* as well (Pan et al., in review), making it an ideal candidate to study the impact of solar exposure on the fluorescence signature of *B. anthracis*. Figure 15 shows a three dimensional plot of the particle size distribution and fluorescence (observed by the UV-APS) of the *B. thurengiensis* used for these experiments. The measurement was taken near the end of aerosol generation during the UV exposure experiment. The peak of the aerosol distribution is approximately at the 1.715 micron bin of the UV-APS. The particle fluorescence intensity increases as a function of size, but does not saturate in the UV-APS.

For the purposes of examining the decay in fluorescence over time, the mean concentration weighted fluorescence was calculated in the 1.715 micron bin and tracked over the course of measurements when particles were exposed to light from the metal halide lamps to simulate solar exposure and with the lights off. Results of these calculations are shown in Figure 16. Based on these measurements, the fluorescence of *B. thurengiensis* is dramatically and rapidly affected exposure to UV light intended to simulate solar exposure. Although there is an increase in the noise (due to a decrease in particle concentration, as discussed above) at the second measurement time, the decrease in fluorescence is readily apparent after only 36 minutes of exposure, particularly when compared to the dark experiments. By the time the final measurement was made at 53 minutes, there were almost no fluorescent particles remaining. This observation is consistent with the author's data from several years of experiments using UV transparent outdoor chambers. Figure 17 shows data from October 2012, taken for the Defense Threat Reduction Agency (DTRA), where *B. thurengiensis* aerosol was exposed to ambient conditions (including sunlight) at Adelphi, MD over periods ranging from a 3 to 5 hours. The rapid drop in fluorescence intensity excited at 355 nm compares relatively well to this laboratory data. Although these data can't be directly compared to the laboratory data since other factors were shown to contribute to the observed loss of fluorescence, and the solar intensity measured in the field was integrated over the entire solar spectrum and the data in the laboratory was only integrated over the UV spectrum, analysis indicated that solar exposure was likely to be the dominant factor in this observed decay. Field data also indicated that while fluorescence intensity is related to viability/infectivity in organisms like viruses, spores (like *B. thurengiensis*) are not necessarily killed by UV radiation as quickly as their fluorescence signatures are modified.

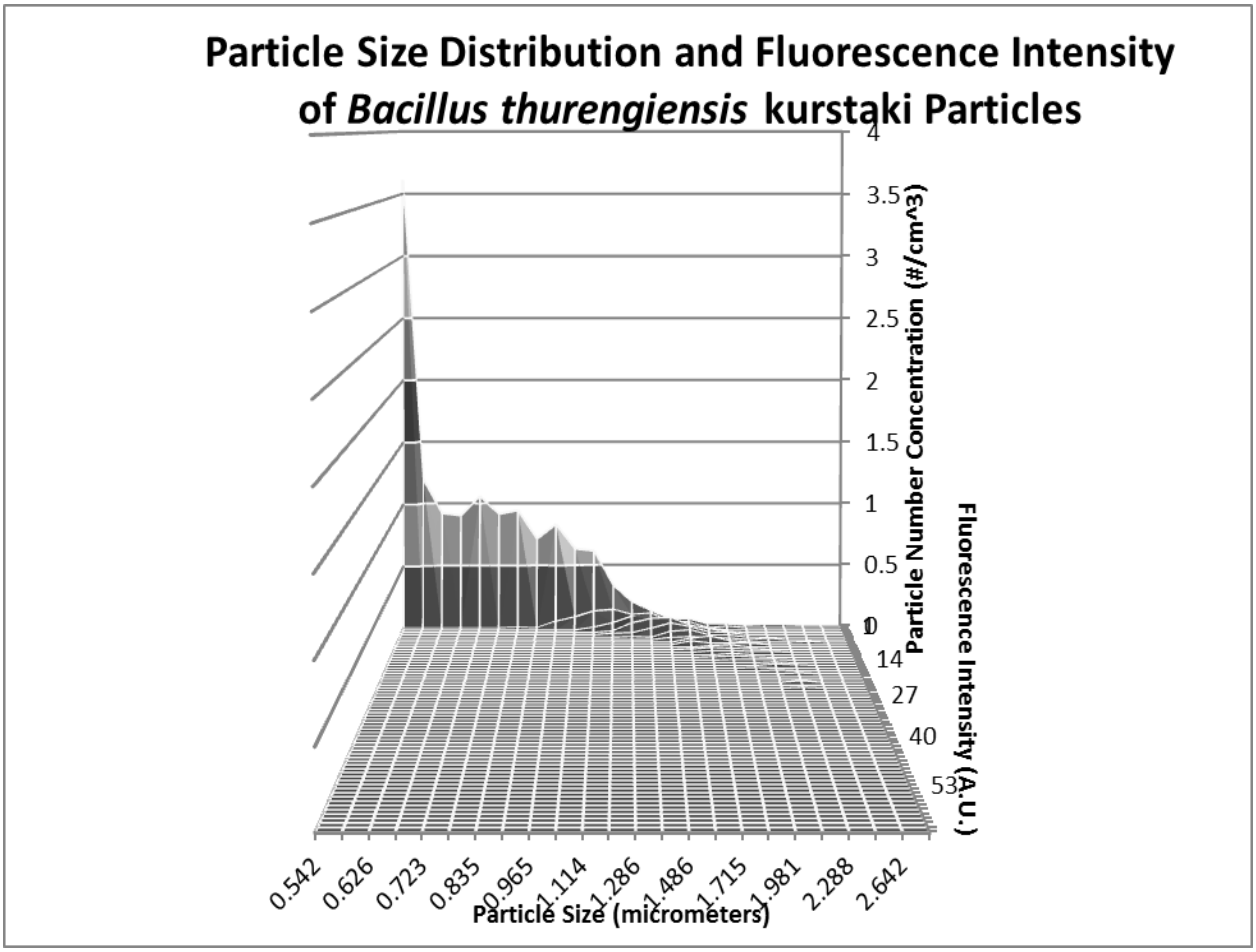

Figure 15. Aerosol number distribution and size resolved integrated fluorescence intensity as measured by the UV-APS for *Bacillus thurengiensis* Kurstaki particles.

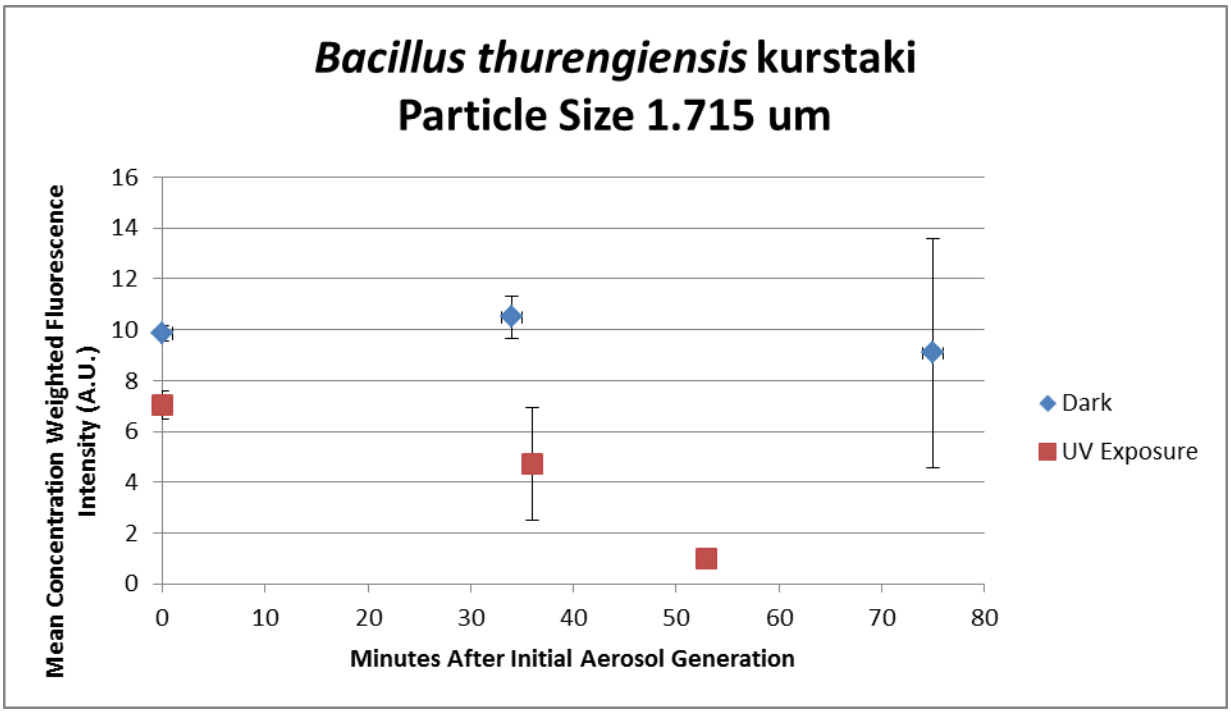

Figure 16. Fluorescence of *BtK* after exposure to simulated sunlight in the rotating drum. The degradation in fluorescence intensity is readily apparent after only a little more than 30 minutes in the drum, and is nearly gone by the last measurement. During the same period, the BtK particles in the dark show no significant change in fluorescence.

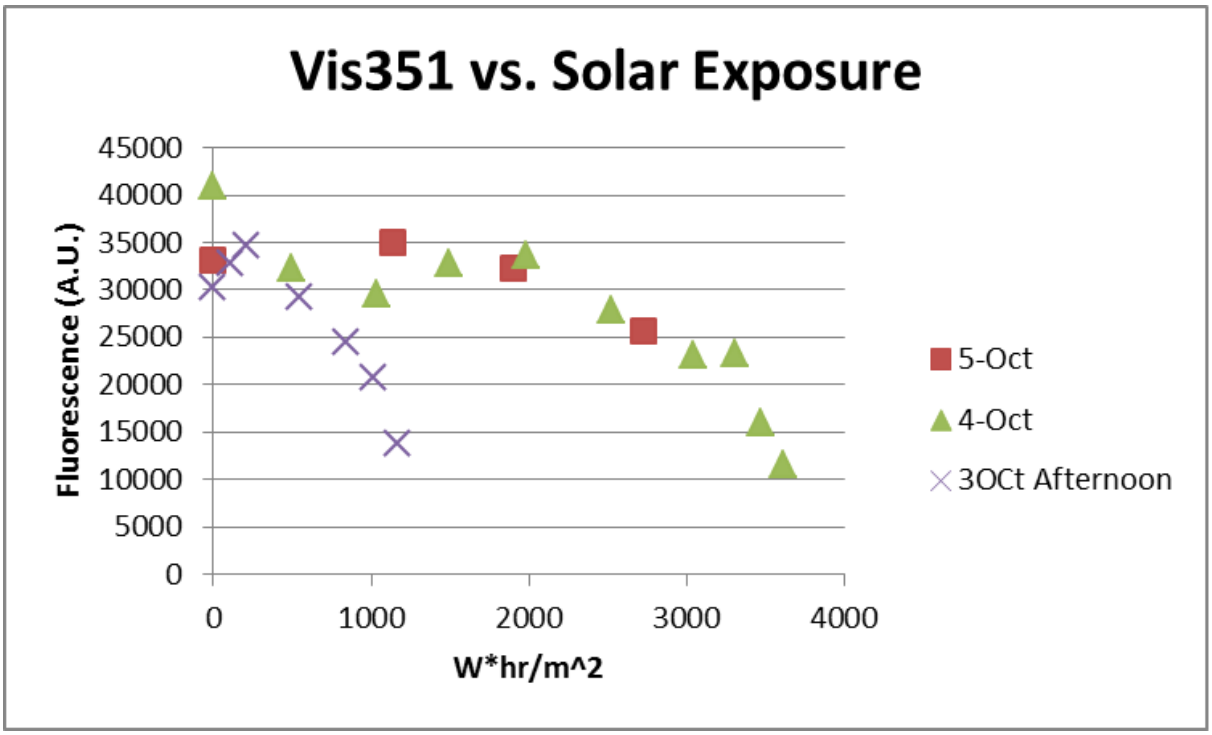

Figure 17. Degradation of fluorescence of BtK under ambient conditions in Adelphi, MD during October of 2012 (from author's unpublished data). Although not directly comparable to the drum data, the data show similar to that seen in the laboratory system.

4. CONCLUSIONS AND FUTURE DIRECTIONS

A laboratory system was constructed that allows the super-micron particles to be aged for long periods of time under conditions that can simulate a range of natural environments and conditions, including relative humidity, oxidizing chemicals, organics and simulated solar radiation. Modeling indicates that despite the changes to the ideal rotating drum design that allow continuous replenishment of reactive chemicals during an experiment, that analytical solutions that have been previously derived for rotating drum chambers still apply to this chamber. Two proof-of-concept experiments using a non-biological simulant for biological particles and a biological simulant demonstrate the utility of these types of aging experiments. While green Visolite®, which is often used as a tracer material for model validation experiments, does not degrade with exposure to simulated solar radiation, the actual biological material does. This would indicate that Visolite® should be a good tracer compound for mapping the extent of a biological release using fluorescence as an indicator, but that it should not be used to simulate the decay of a biological particle when exposed to sunlight. It is also encouraging that decay in the fluorescence measured for *B. thurengiensis* is similar to what has been previously observed in outdoor environments.

Further improvements to the rotating drum system need to be made in order to perform more complicated experiments. Improved control over relative humidity is necessary to maintain control over high humidity experiments when the ambient humidity is extremely low. Further, while the system design is flexible enough to allow generation of photochemical precursors, such as NOx and terpenes, we have yet to demonstrate that urban photochemistry can be initiated in the chamber using the simulated solar radiation and precursors alone. Additional metal halide bulbs should also be added to the system to increase the intensity of simulated solar radiation that can be used in the system. These improvements and further experiments will continue under funding from the DTRA.

5. REFERENCES

Andereck, C.D., et al. (1986). Flow regimes in a circular Couette system with independently rotating cylinders. *J. Fluid Mech*. 164: 155-183.

Asgharian, B., and Moss, O.R. (1992). Particle suspension in a rotating drum chamber when the influence of gravity and rotation are both significant. *Aerosol Sci. Tech*. 17:263-277.

Cox, C. S., A. M. Hood, and Jean Baxter. "Method for Comparing Concentrations of the Open Air Factor." *Applied Microbiology* 26 (1973): 640-42.

Dark, F. A., and T. Nash. "Comparative toxicity of various ozonized olefins to bacteria suspended in air." *J. Hyg.* 68 (1970): 245-252.

Goldberg, L. J., Watkins, H. M. S., Boerke, E. E., and Chatigny, M. A., (1958). The use of a rotating drum for the study of aerosols over extended periods of time. *Amer. J. Hyg*. 68, 85-93.

Gruel, R.L., Reid, C. R., and Alleman, R. T., (1987). The optimum rate of drum rotation for aerosol aging. *J. Aerosol Sci*. 18, 17-22.

Kriebel, A.R. (1961). Particle Trajectories in a Gas Centrifuge. *J. Basic Eng*. 333-340.

Krumins, V., E.-K. Son, G. Mainelis, D.E. Fennell, (2008). Retention of Inactivated Bioaerosols and Ethene in a Rotating Bioreactor Constructed for Bioaerosol Activity Studies. *Clean*, 36, 593-600.

Lapple, C.E., and Shepherd, C.B. (1940). Calculation of Particle Trajectories. *Ind. Eng. Chem*. 32:605-617.

Pan, Y.-L., J.L. Santarpia, S. Ratnesar-Shumate, E. Corson, J. Eshbaugh, S. C. Hill, C. C. Williamson, M. Coleman, C. Bare, S. Kinahan, (2013). Effects of ozone and relative humidity on fluorescence spectra of octapeptide bioaerosol particles, *Journal of Quantitative Spectroscopy and Radiative Transfer*, 133, 538-550.

Rayleigh, O.M. (1917). On the Dynamics of Revolving Fluids. *Roy. Soc. Proc. A.* 93: 148-154.

Santarpia, J.L., Y. Pan, S. Hill, N. Baker, B. Cottrell, L. McKee, S. Ratnesar-Shumate, and R. Pinnick, (2012). Changes in fluorescence spectra of bioaerosols exposed to ozone in a laboratory reaction chamber to simulate atmospheric aging. *Opt. Express*, 20, 29867-29881.

Taylor, G.I. (1923). Stability of a Viscous liquid contained between two rotating cylinders. *Phil. Trans. Roy. Soc. London.* 223: 605-615.

6. DISTRIBUTION

4 Lawrence Livermore National Laboratory
Attn: N. Dunipace (1)
P.O. Box 808, MS L-795
Livermore, CA 94551-0808

1	MS1135	Brandon Servantes	01532
1	MS1148	Gabriel Lucero	06633
1		Andres Sanchez	06633
1		Josh Hubbard	06633
1		Josh Santarpia	06633
1	MS0782	Paul Smith	06633
1	MS0899	Technical Library	9536 (electronic copy)
1	MS0359	D. Chavez, LDRD Office	1911


Sandia National Laboratories